IEEE Access
Multidisciplinary | Rapid Review | Open Access Journal

Received November 19, 2017, accepted January 6, 2018, date of publication January 16, 2018, date of current version February 28, 2018.

Digital Object Identifier 10.1109/ACCESS.2018.2794340

A Fast Single-Image Dehazing Method Based on a Physical Model and Gray Projection

WENCHENG WANG[1], (Member, IEEE), FALIANG CHANG[2], TAO JI[1], AND XIAOJIN WU[1]
[1]College of Information and Control Engineering, Weifang University, Weifang 261061, China
[2]College of Control Science and Engineering, Shandong University, Jinan 250100, China

Corresponding author: Wencheng Wang (wwcwfu@126.com)

This work was supported in part by the National Natural Science Foundation of China under Grant 61403283 and Grant 61673244, and in part by the Shandong Provincial Natural Science Foundation under Grant ZR2013FQ036 and Grant ZR2015PE025.

ABSTRACT Due to the scattering of atmospheric particles, images captured under hazy conditions suffer from contrast attenuation and color distortion, which severely affect the performance of machine vision systems. Various types of methods have been developed to improve the clarity of images. However, these methods are typically challenging to apply in real-time systems. We present a fast, single-image dehazing method based on the atmospheric scattering theory and dark channel prior theory. The transmission map is approximately estimated using a fast average filter, the subsection mechanism is designed to avoid the high brightness of the sky region in the recovered image, the region projection method is adopted to obtain the atmospheric light, and image color compensation is implemented using the Weber–Fechner law. Our experimental results show that this algorithm can restore images to a clear and natural state and ensure the balance of quality and the speed of image restoration. Therefore, the algorithm can be used in real-time systems.

INDEX TERMS Gray projection, image dehazing, subsection mechanism, transmission estimation.

I. INTRODUCTION

In hazy conditions, the scattering of atmospheric particles leads to severe degradation of the information captured by optical sensors. The contrast and fidelity of the image are attenuated to different degrees, which directly affects the visual perception of human operators and the performance of the machine vision system [1], [2]. Therefore, it is important to investigate methods of image dehazing. Generally, such methods are divided into the image-enhancement-based method and image-restoration-based method. The first class aims to improve the image visual effects by enhancing the contrast of hazy images, including histogram equalization [3], Retinex [4], homomorphic filtering [5], and wavelet transform [6], among other methods. These methods can enhance the visual effect of the image but do not reliably remove the haze. In the image-restoration-based method, a physical model is established for the degradation of the hazy image, and the lost information is compensated with the inversion algorithm. This method has the natural effect of dehazing and has received considerable recent attention [7]. For example, Narasimhan and Nayar [8] obtained approximate depth information by artificially specifying the maximum and the minimum depth of field. They then recovered a clear image based on the physical model. Hautiere *et al*. [9] used a vehicle-mounted optical sensor system to calculate the depth of the scene and applied a 3-D geography model to dehaze the images. Kopf *et al*. [10] used a map to provide the basic terrain, constructed a 3-D model of the scene from known depth and texture information, and then used a model to achieve dehazing. This method is based on the premise that depth information for the scene is known and can be used to perform reliable image restoration. Subsequently, Schechner *et al*. [11] used the polarization characteristics of sky brightness to capture multiple images of the same scene at different polarization angles and then reconstructed the degraded image with depth information by estimating the degree of polarization. Nayar and Narasimhan [12] obtained the depth information of a scene and restored the image by capturing two images in different weather conditions, which achieved satisfactory results. Both algorithms require multiple images for post processing, however, and it is often challenging to obtain multiple images of the same scene under different conditions in practice, hindering the application and popularization of these approaches.

In recent years, single image-dehazing algorithms based on a certain hypothesis or prior knowledge have garnered

significant attention. For example, Tan [13] achieved image dehazing by maximizing the contrast of the restored image based on the prior knowledge that the haze-free image had a higher contrast than the hazy image. However, this approach can easily lead to oversaturation. Fattal [14] assumed that the surface chromaticity of the object was not statistically correlated with the propagation of the medium and used independent component analysis to estimate the albedo of the scene. This method can produce satisfactory results when the haze is thin but fails for thick hazy images because of the lack of color information. He *et al*. [15] proposed a dehazing method based on the dark channel prior (DCP). This process uses a minimum filter to estimate and optimize the transmission map of the media, which is designed from the statistics of a haze-free image database and achieves satisfactory results. Tarel and Hautière [16] used a median filter to estimate the atmospheric transmission function and then applied a tone map to obtain the dehazed image. The algorithm recovered the image clearly and vividly but caused a halo effect from the depth-of-field mutation. Kratz and Nishino [17] assumed that the hazy image was composed of two separate layers: the scene albedo and the scene depth. They ultimately achieved relatively accurate depth information using the factorial Markov random field (FMRF). However, the color in the image obtained by this method was too saturated. Subsequently, Ancuti and Ancuti [18] proposed a method based on image fusion, Wang and Feng [19] proposed a dehazing algorithm based on transmittance fusion, Gibson and Nguyen [20] presented a fast, single-image dehazing algorithm using adaptive Wiener filtering, Meng *et al*. [21] proposed an efficient regularization method for single-image dehazing, Kim *et al*. [22] proposed a cost function method based on image contrast and the degree of lost information, Fattal [23] proposed a color-based method, and Zhu *et al*. [24] proposed a prior color attenuation to create a linear model.

Among the above algorithms, the DCP method proposed by He *et al*. [15] has been widely investigated because of its simple principle and superior results. However, the method uses soft-matting to refine the transmission map, which requires high computational costs. A variety of methods have been developed to accelerate the transmission map refinement, such as bilateral filtering [25], [26], guided filtering [27], anisotropic filtering [28], edge-preservation filtering [29], and median filtering [30], which are challenging to implement in real-time systems [31]. In addition, the sky region and white objects do not meet the prior dark channel assumption, which results in a block effect or severe color distortion in the restored image.

We propose an improved algorithm based on the DCP to address the fact that the current dehazing method is ineffective for sky regions and that the processing time is excessively long. The algorithm obtains the transmission map through a simple and fast average filtering process to improve the running speed. By segmenting the calculations, we eliminate block effects and color distortion. In addition, to address the phenomenon of image dimming after restoration, color remapping is performed to increase the visual effect of the image. The algorithm achieves a certain degree of dehazing and reduces the processing time, which has application value.

The remainder of this paper is organized as follows. Section 2 briefly introduces the atmospheric scattering model. In Section 3, the key steps are described, including the principle of sky segmentation, the method to obtain atmospheric light using the quad-tree, the fusion principle of the transmission map and the method of image restoration. Section 4 presents the experimental results, and Section 5 concludes this work.

II. RELATED WORK

A. ATMOSPHERIC SCATTERING MODEL

According to the theory of atmospheric scattering, an imaging model of a hazy scene consists primarily of two parts, which is shown in Figure 1. The first part is the attenuation process of the reflected light from the object surface to the camera. The second part is the scattering of air-light reaching the camera. Both parts constitute the theoretical basis of blurred hazy images.

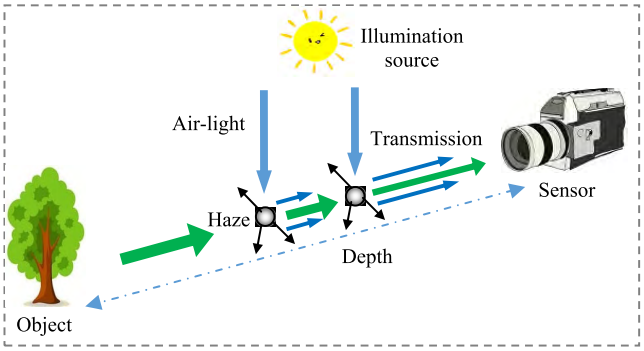

FIGURE 1. Atmospheric scattering model.

Therefore, in the field of computer vision, the scattering model to describe hazy images can be expressed as

$$I(x) = J(x)t(x) + A(1 - t(x)) \tag{1}$$

where x is the distance coordinate, $I(x)$ is the hazy image, $J(x)$ is the haze-free image, A is the atmospheric light, and $t(x)$ is the transmission rate of the medium. The purpose of image dehazing is to recover $J(x)$ from $I(x)$.

The degradation model has several unknown parameters, resulting in an ill-posed problem. Only after estimating the parameters A and $t(x)$ can $J(x)$ be restored from $I(x)$.

B. DCP THEORY

The DCP theory originates from the statistics of haze-free images [13]. That is, in most non-sky local regions, at least one color channel has a low value in some pixels that tend to zero, which can be expressed as follows:

$$J^{dark}(x) = \min_{c\in\{r,g,b\}} \left(\min_{y\in\Omega(x)} (J^c(y)) \right) \to 0 \tag{2}$$

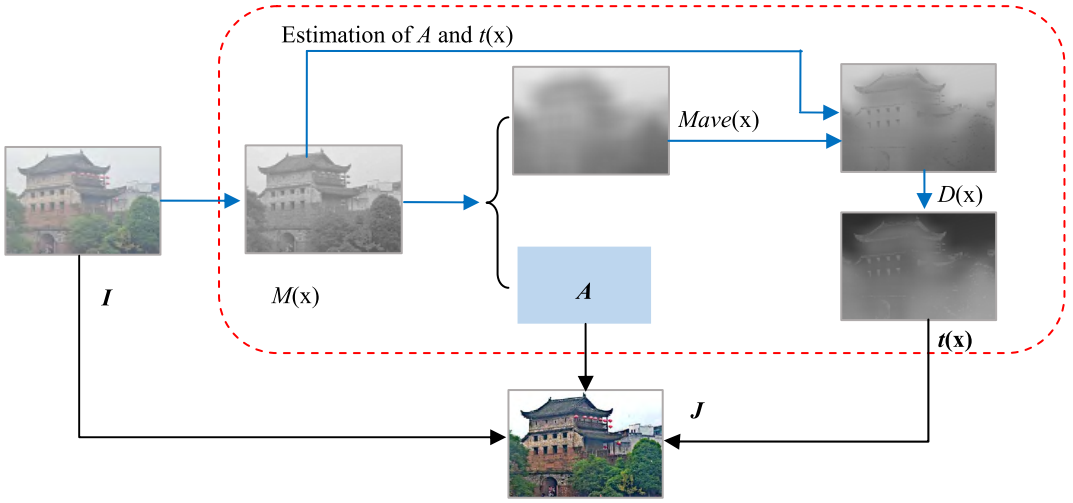

FIGURE 2. Framework of the image-dehazing algorithm.

where J^c is one color channel of J, $\Omega(x)$ is a small block centered at x, and J^{dark} is the dark channel image.

To estimate the transmission rate $t(x)$, we assume that the atmospheric light A is known and that the transmission rate $\tilde{t}(x)$ in the local region $\Omega(x)$ is constant. If both sides of Eq. (1) are simultaneously divided by A^c, then $\min_{c\in\{r,g,b\}}(\min_{y\in\Omega(x)}())$ is transformed, and the $\tilde{t}(x)$ is obtained according to Eq. (2).

$$\tilde{t}(x) = 1 - \min_{c\in\{r,g,b\}}(\min_{y\in\Omega(x)}(\frac{I^c(y)}{A^c})) \tag{3}$$

In practice, to ensure that the image retains a sense of depth, a correction factor $\omega(0 < \omega \leq)$ is introduced to maintain partial haze. Then, Eq. (3) can be re-formulated as follows:

$$\tilde{t}(x) = 1 - \omega \min_{c\in\{r,g,b\}}(\min_{y\in\Omega(x)}(\frac{I^c(y)}{A^c})) \tag{4}$$

The block effect typically exists in the transmission map due to the assumption that the regional transmission is constant. Then, soft-matting or guided filtering [15] is used to refine $t(x)$.

According to the atmospheric scattering model, once the transmission map $t(x)$ and the atmospheric light A are obtained, the scene depth can be restored according to Eq. (1):

$$J(x) = \frac{I(x) - A}{t(x)} + A \tag{5}$$

The estimation method of the atmospheric light A is to first find the top 0.1% of pixels with the largest brightness in J^{dark} and then to select the maximum value of the pixels that correspond to the pixels in the original image.

C. DEFECTS OF DCP

The algorithm proposed by He *et al.* [15] has the following limitations:

(1) The method uses soft-matting to refine the transmission map, which typically results in slow computing speed. Although a variety of methods have been developed to accelerate the transmission map, refinements such as bilateral filtering [25], [26], guided filtering [27], anisotropic filtering [28], edge-preserving filtering [29], median filtering [30] and linear models [31] are still challenging to implement in real-time systems.

(2) The method cannot be applied to white regions, such as sky and water surfaces, due to the assumption of the DCP because the dark channel values of these regions $J^{dark}(x)$ are non-zero. That is,

$$t(x) = [1 - I^{dark}/A] < [1 - I^{dark}/A]/[1 - J^{dark}/A] \tag{6}$$

Thus, the transmission map estimated using the DCP-based algorithm is limited to the bright areas, which results in a significant enlargement of the slight difference between the pixel channels in the sky region after being divided by a relatively small t (as given by Eq. (4)). As a result, the color of the restored image is distorted.

III. FAST DEHAZING METHOD

To address the above problems, we designed a fast dehazing algorithm based on the DCP theory and gray projection in this paper. The algorithm reduces the operational complexity, ensures a successful dehazing effect, and can be applied to real-time systems. This method is divided into three steps. (1) Estimation of the transmission map. Minimum filtering and fast average filtering are performed on the original image, and the white region is compensated by piecewise processing. (2) Estimation of the atmospheric light. Gray projection is used to segment the sky region and calculate the atmospheric light. (3) Image restoration. The atmospheric scattering model is used for image recovery, and the Weber-Fechner Law is selected to adjust the brightness. The entire process of the dehazing algorithm is shown in Figure 2.

FIGURE 3. Estimation of transmission map. (a) Hazy image. (b) Minimum filtering. (c) Average filtering. (d) Grayscale optimization.

A. ESTIMATION OF TRANSMISSION MAP

The steps of the algorithm are as follows:

(1) Minimum Filtering

To avoid the block effect caused by the transformation of $\min_{c\in\{r,g,b\}}()$ in the local region, the minimum of the three color channels is selected using the following formula:

$$M(x) = \min_{c\in\{r,g,b\}}(I^c(x)) \tag{7}$$

where x is a pixel in the image.

However, this calculation roughens the transmission map. As shown in Figure 3(b), the results are rich in edge information, and the luminance value does not accurately represent the haze density. Therefore, it is necessary to further eliminate the unnecessary texture information and the influence of white objects in $M(x)$.

(2) Fast Average Filtering

To smooth $M(x)$ and avoid the grayscale jump between neighboring pixels, average filtering is required, which is expressed as

$$M_{ave}(x) = average_{\lambda}(M(x)) \tag{8}$$

where λ is the size of the filter window, which is set at 1/20 of the image's width.

To improve the computing speed [32], the integral image is used. For the input image i, the integral image $ii(x, y)$ at the pixel (x, y) is defined as

$$ii(x, y) = \sum_{x'\le x}\sum_{y'\le y} i(x,' y') \tag{9}$$

where $i(x,' y')$ is the gray value of pixel $(x,' y')$.

The sum of the pixels within an arbitrary rectangle can be obtained using the following operations:

$$ii(x, y) = ii(x-1, y) + ii(x, y-1) - ii(x-1, y-1) + i(x, y) \tag{10}$$

As shown in Figure 4, the integral image $ii(x, y)$ is equal to the sum of all the pixels in the gray portion of the image.

Thus, for all pixels in a rectangular region D, the grayscale integral is

$$Sum(D) = ii_4 + ii_1 - (ii_2 + ii_3) \tag{11}$$

In this paper, a box filter is used to increase the calculation speed by a factor of four based on the integral image.

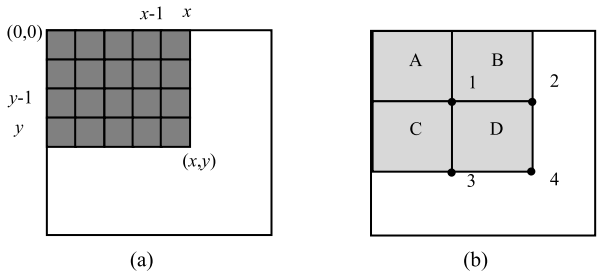

FIGURE 4. Calculation of the integral image. (a) Integral value of point (x, y). (b) Integral calculation of rectangle D.

In contrast, the data stored in the matrix are directly the sum of the current pixel and its neighbors. The corresponding element in the matrix can then be directly accessed, and the computational complexity is $O(1)$.

(3) Grayscale optimization. The result of the mean filtering can reflect the trend of the gray in the image. However, a gap remains within the real value that must be compensated as follows:

$$D(x) = \min(A \times M_{avg}(x), M(x)) \tag{12}$$

(4) If the atmospheric light A is known, then the transmission map can be calculated using Eq. (3). In practice, to retain a partial haze to give the image a sense of depth, the correction factor $\omega(0 < \omega \le)$ is introduced. Then, Eq. (3) can be re-formulated as

$$\tilde{t}(x) = 1 - \omega\frac{D(x)}{A} \tag{13}$$

B. ESTIMATION OF ATMOSPHERIC LIGHT

Another key factor in solving the hazy imaging in Eq. (3) is the estimation of the atmospheric light A. According to the haze characteristics, significant haze will increase the brightness of the object. Therefore, Tan [13] took the maximum value of the hazy image as the atmospheric light A. In the He *et al.* [15] method, the highest original pixel values of the top 0.1% brightest pixels in the DCP images were regarded as the atmospheric light A. However, when a white object exists in the scene, if the window selection during the dark-channel image acquisition is not appropriate, the white object will remain and cause the selected atmospheric light intensity to be based predominantly on this object. Thus, the atmospheric

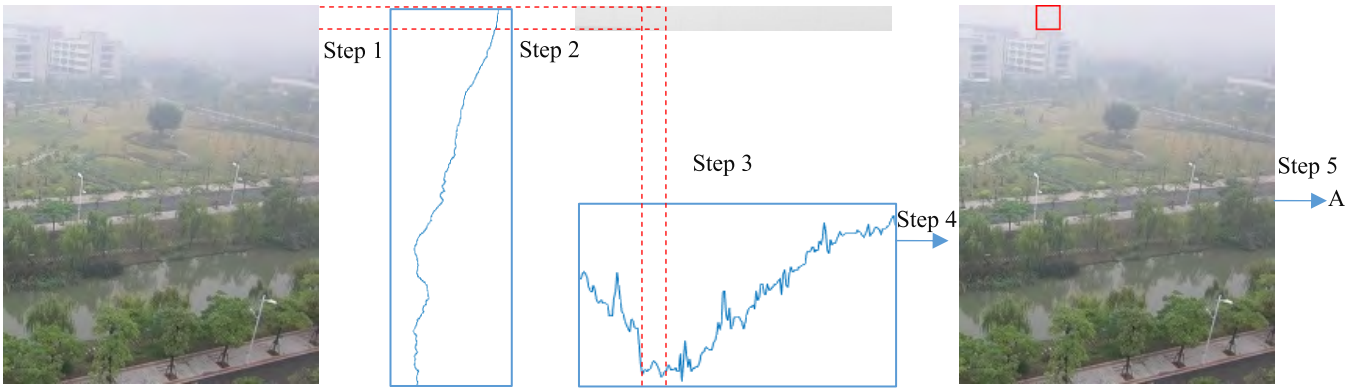

FIGURE 5. Calculation of atmospheric light.

light values obtained by the above two methods often deviate from the actual situation. For example, Kim *et al.* [22] used the maximum regional mean as the condition for quad-tree decomposition. This approach can obtain the sky sub-region but often fails for a white object in the region.

In outdoor images, the sky portion generally has the characteristics of large area, bright color and smoothness. Therefore, to find pixels with high brightness and smoothness, the gray projection method is used for location isolation. The main steps are as follows:

Step 1: Horizontal projection of the minimum filtered image. Assuming that the size of input image $I(x, y)$ is $m \times n$ pixels, the horizontal projection is expressed as

$$H(y) = \sum_{x=1}^{m} I(x, y) \quad 1 \le x \le m \tag{14}$$

Step 2: Sum the horizontal projection with a width of $2b+1$ pixels, and select the maximum region as follows:

$$H_{\max} = \max\left(\sum_{y=s-b}^{s+b} H(y)\right) \quad b+1 \le s \le m-b \tag{15}$$

The maximum region is saved as an image $K(x, y)$ with a size of $(2b+1) \times n$ pixels.

Step 3: Vertical projection is conducted on $K(x, y)$, and the formula is expressed as

$$V(x) = \sum_{x=1}^{n} K(x, y) \quad 1 \le y \le 2b+1 \tag{16}$$

Step 4: Sum the value of the vertical projection with a width of $2b+1$ pixels, and select the maximum region as follows:

$$V_{\max} = \max\left(\sum_{x=s-b}^{s+b} V(x)\right) \quad b+1 \le s \le n-b \tag{17}$$

The maximum region is saved as an image $R(x, y)$ with a size of $(2b+1) \times (2b+1)$ pixels.

Step 5: Calculate the atmospheric light. The pixel values that belong to the sky region are extracted first. Then, the pixel values are arranged in descending order. Finally, the average gray values of the top 1% pixels with the largest brightness values are selected as the atmospheric light value A, expressed as follows:

$$A = mean(\max^{0.1} R(x)) \tag{18}$$

The maximum gray of the hazy region obtained by this method is indicated by a white mark 1. Experimental results show that this method can offset the influence of the white clouds in the sky region to some extent and can eliminate the estimation bias caused by the salt-and-pepper noise that may exist in the image. The process is illustrated in Figure 5.

After the projection, we perform a repeated summed calculation over a certain region, using the box filter acceleration algorithm to improve the computing speed. Assuming that the data column is $i(x)$ $(1 \le x \le n)$ and the region width is $(2b+1)$, the sum of the regions is given by

$$Sum(t) = \sum_{x=t-b}^{t+b} i(x) \quad b+1 \le t \le n-b \tag{19}$$

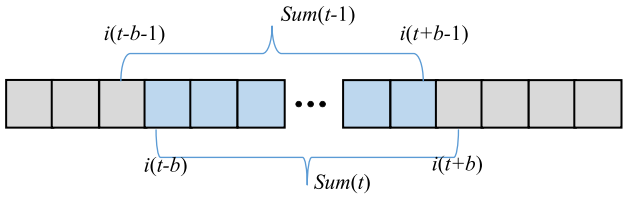

FIGURE 6. Acceleration with box filter.

As shown in Figure 6, since a total number of $2b$ duplicate points $\{i(t-b+1), i(t-b+2), \ldots i(t+b-1)\}$ exist in the adjacent regions $Sum(t-1)$ and $Sum(t)$, those values can be calculated using the former results as follows:

$$Sum(t) = Sum(t-1) - i(t-b) + i(t+b) \quad b+1 \le t \le n-b \tag{20}$$

Using the acceleration, $(2b+1)$ operations can be reduced to three operations, which greatly improves the computing speed.

C. CALCULATION OF THE TRANSMISSION MAP

The DCP assumption is insufficient in the highlighted region, which causes the transmission rate to be small and close to zero, resulting in color distortion [33], [34]. In this study, we segmented the sky and non-sky regions of the image to distinguish the bright areas and the non-bright areas from the hazy image.

We first calculate the maximum difference $\Delta_{\max}(x)$ between the three RGB channels and the atmospheric light A and label this difference as follows:

$$\Delta_{\max}(x) = \max_{c\in\{r,g,b\}} \{\left|I^c(x) - A\right|\} \tag{21}$$

If the maximum value of the three channels is close to the threshold value T, i.e., if $\Delta_{\max}(x) < T$, then this region is considered a bright area. Otherwise, it is considered a non-bright area. The transmission map $t(x)$ at each point in the bright area is corrected as follows:

$$t_2(x) = \begin{cases} t(x) & \Delta_{\max}(x) \geq T \\ \min\left(\dfrac{T}{\Delta_{\max}(x)} \cdot t(x), 1\right) & \Delta_{\max}(x) < T \end{cases} \tag{22}$$

where $t(x)$ is the transmission map after the average filtering process. We found through experimentation that when T is set to 0.2, the evaluation of the sky region is more accurate and produces an improved effect. However, the threshold value T is a constant determined by experience and cannot be applied to different images. Because of the large differences between the average gray and sky brightness of the image with a small bright area, we designed a method based on the statistics of the atmospheric light and average gray to define an adaptive threshold. In this way, a more accurate transmission distribution of the bright area can be obtained. The formula is expressed as follows:

$$T = \begin{cases} 0.15 & (A - I_m) \leq 0.25 \\ A - I_m - 0.1 & 0.25 < (A - I_m) < 0.35 \\ 0.25 & (A - I_m) \geq 0.35 \end{cases} \tag{23}$$

$$I_m = mean(I(x)) \tag{24}$$

where I_m is the average gray of the entire image, *mean* is the average operation, and A is the sky brightness.

The proposed method can accommodate hazed images with large bright areas without any departure from the DCP assumption. This modification introduces limited changes on the original algorithm.

Figure 7(a) and 7(b) show the transmission maps before and after the correction. The corresponding dehazed images are shown in Figure 7(c) and 7(d). The corrected transmission has an improved effect on the bright areas, without color distortion.

D. IMAGE RESTORATION AND TONE ADJUSTMENT

After the transmission map $t(x)$ and the atmospheric light A have been computed, the haze-free image of the scene under ideal conditions can be directly restored using Eq. (5).

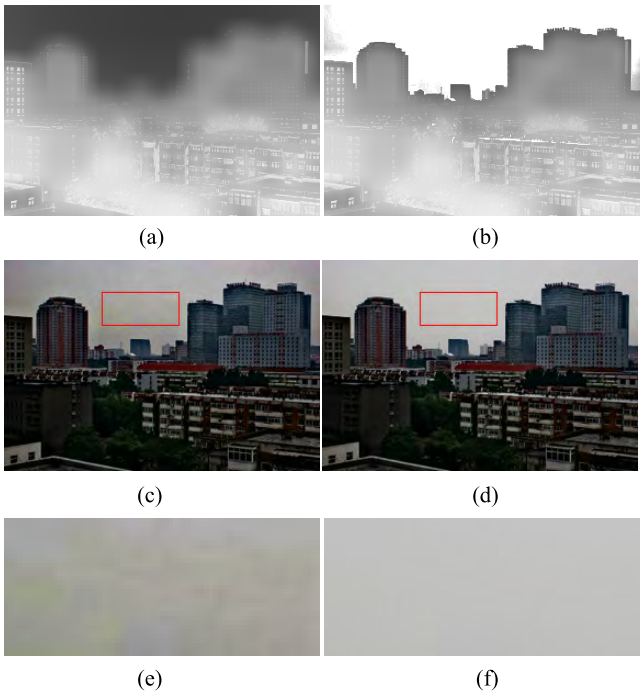

FIGURE 7. Comparison of the image before and after correction. (a) Transmission map. (b) After correction of (a). (c) Restored image with (a). (d) Restored image with (b). (e) Magnification of rectangle (c). (f) Magnification of rectangle (d).

When $t(x)$ approaches zero, the direct attenuation term also approaches zero. This relation excessively increases the dehazed image pixel values. The restored image may contain noise; thus, a lower bound $t_0 = 0.1$ is set for the transmission map $t(x)$, making the dehazing effects appear more natural. The final dehazing image J is expressed as

$$J(x) = \frac{I(x) - A}{\max(t(x), t_0)} + A \tag{25}$$

In addition, since the image is affected by the surrounding environment and lighting on hazy days, parts of the images may have a low brightness, and the restored images based on the DCP will be even darker. According to the Weber-Fechner Law [35], the subjective brightness perceived by the human eye is acquired by nerve stimulation from light reflected from the object shining on the retina. The subjective brightness L_d and the objective brightness L_0 present a logarithmic linear relationship as follows:

$$J_d = \beta \lg(J) + \beta_0 \tag{26}$$

where β and β_0 are constants. The relationship between the subjective brightness and the objective brightness is shown in Figure 8(a) and is used to adjust the tone of the restored images. To avoid the increased computation complexity from the logarithm operation, in the actual application of this method, a simple function is adopted to match Figure 8(a) with the following expression:

$$J_d = \frac{J(255 + k)}{J + k} \tag{27}$$

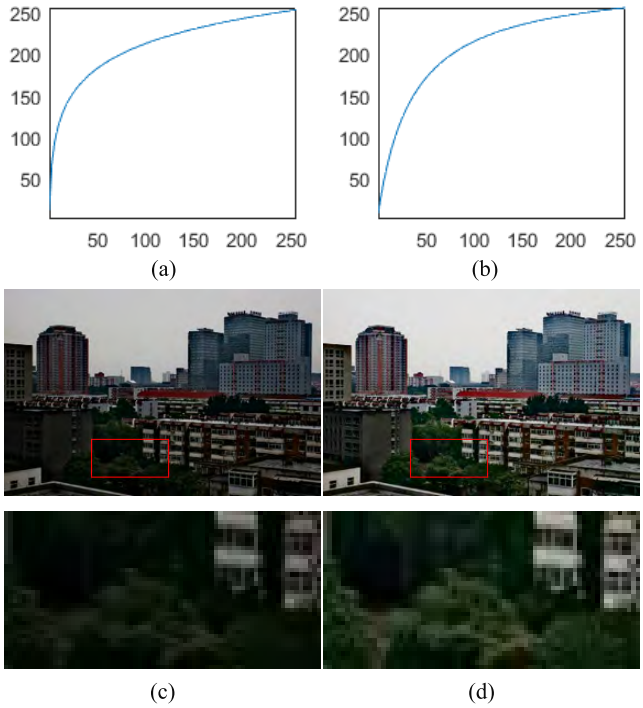

FIGURE 8. Adjustment curve of brightness. (a) Weber-Fechner law. (b) Adjusted curve. (c) Before adjustment. (d) After adjustment.

where k is the adjustment coefficient. The smaller the adjustment coefficient, the greater the degree of adjustment. The adjustment curve is shown in Figure 8(b) below.

In the experiment, k is automatically obtained according to the average gray of the image, and its value is calculated using $k = 1.5 \times I_m$. An image comparison before and after the adjustment is shown in Figure 8(c) and 8(d), where the lower images are the magnified areas of the rectangles. In Figure 8(c), although the haze is removed, the overall brightness is poor, giving the image a dark tone. Relative to Figure 8(c), the overall brightness and contrast of the adjusted image in Figure 8(d) is improved, and the visual effects are closer to the actual scene that would be seen under more favorable weather conditions.

E. STEPS OF THE ALGORITHM

Combined with the principle of DCP and the improvement strategies, the specific steps for the image processing are as follows:

(1) The hazy image $I(x)$ is input.

(2) Based on Eq. (7), the minimum filter is used on $I(x)$ to obtain the DCP image $M(x)$.

(3) Based on Eq. (8), $M(x)$ is operated on by an averaging filter to obtain the smoothed image $M_{ave}(x)$.

(4) Based on Eq. (12), $M_{ave}(x)$ is compensated by a grayscale filter to obtain the corrected image $D(x)$.

(5) The atmospheric lighting information is automatically obtained using the projection method, and the atmospheric light intensity A is generated.

(6) Based on Eq. (13), the initial transmittance $\tilde{t}(x)$ is calculated.

(7) The transmission map is adaptively modified using the segmentation mechanism to obtain $t(x)$.

(8) The image is restored based on the physical model in formula (25) to obtain the restored image $J(x)$.

(9) The brightness compensation is performed on the restored image based on Eq. (27), and the image $J_d(x)$ is obtained.

(10) The image $J_d(x)$ is output.

IV. ANALYSIS OF EXPERIMENTAL RESULTS

To test the effectiveness of the dehazing algorithm, we built an experimental platform and compiled the algorithm into a program. In this experimental configuration, the hardware is a Dell notebook computer with an Intel(R) i7-5500U 2.4 GHz CPU processor and 8 GB RAM running MATLAB 2014b under Windows 8. The test images are taken from well-known dehazing literature related to city streetscapes, natural landscapes and aerial images, vistas and close-ups. Selected experimental results are shown in Figure 9, in which the names of the eight experimental images are 'Street,' 'Mountain,' 'Cannon,' 'Building,' 'Toys,' 'Road,' 'City' and 'Stadium'. The odd rows show the original images, and the even rows show the restored images. Regardless of the sharp or flat depth-of-field variations, natural and clear restoration results can be obtained under various conditions due to the feasibility and effectiveness of the transmission estimation function. These results also show that the method features strong adaptability to any scene.

To evaluate the advantages of this method, the experimental results are compared with those of classical image enhancement methods, including Fattal's [14] method, He *et al.*'s [15], [27] method, Kim *et al.*'s [22] method, and Zhu *et al.*'s [24] method. The comparison involves subjective evaluation, objective evaluation and computational complexity. The subjective visual evaluation is performed qualitatively, and the objective evaluation index is performed quantitatively.

A. SUBJECTIVE EVALUATION

1) COMPARISON WITH IMAGE-ENHANCEMENT-BASED METHODS

Figure 10 compares the results of the proposed method with that of image-enhancement-based methods. Figure 10(a) shows the hazy image, and Figure 10(b)-10(h) show the dehazed images under the contrast stretching method, histogram equalization, adaptive histogram equalization, the Retinex method, homomorphic filtering, wavelet transform and the proposed method. Figure 10(b)-10(h) exhibit different degrees of changes relative to the original image. In Figure 10(c)-10(e), the visual contrast is significantly enhanced, and the details are clear. However, in Figure 10(g), the hue is dramatically shifted. In Figure 10(b) and 10(f), although the entire tone does not shift, the improvement effect

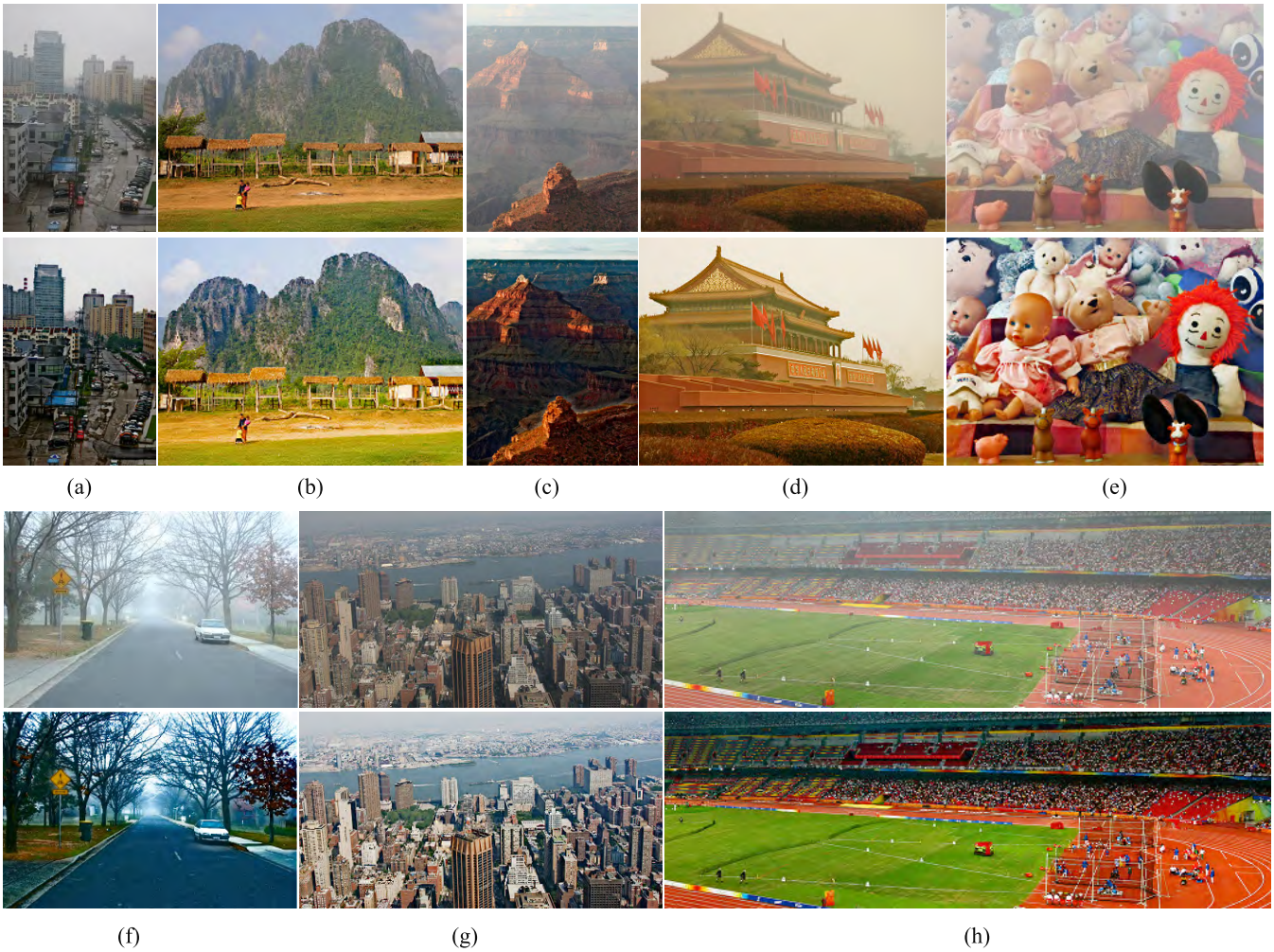

FIGURE 9. Experimental results. (a) Street. (b) Mountain. (c) Cannon. (d) Building. (e) Toys. (f) Road. (g) City. (h) Stadium.

is only minimally detectable. The simple strength stretching leads to a loss of some details, and the homomorphic filtering method leads to dark color. In contrast, the method proposed here, whether in terms of color or details, gives significantly improved results, and the visual effect is superior.

2) COMPARISON WITH IMAGE-RESTORATION-BASED METHODS

In this paper, the 'Pumpkins,' 'Cones,' 'Mountain,' 'People' and 'Hill' images are chosen as the experimental images. The restoration-based processing techniques, including Fattal's method [14], He *et al.*'s [15] method, Kim *et al.*'s [22] method, Zhu *et al.*'s [24] method and Cai's method, are used for qualitative comparisons with the proposed method. The experimental results are shown in Figure 11. Figure 11(a) shows the original image, and Figure 11(b)-11(g) show the results of Fattal's method, He's method, Kim's method, Zhu's method, Cai's method and the proposed method. The visibility and contrast of each dehazed image are greatly improved over that of the original image, and a satisfactory dehazing effect is obtained. For both the 'Pumpkins' and 'Cones' images, Zhu's method is only minimally dehazed, while Kim's method provides satisfactory dehazing but distorts the color. He *et al.*'s [15] method, Fattal's [14] method and the proposed method provide better color recovery than Zhu's method and Kim's method. For the dehazing effect on the 'Hill' image, Kim *et al.*'s [22] method, He *et al.*'s [15] method and the proposed method produce the most appealing results. In terms of the local details of the dehazed image, Kim's method provides outstanding results at close-range, as shown in the third row, but its overall results are inferior to that of the other approaches. Both He's method and Zhu's method can achieve satisfactory performance on far-range and close-range scenes, but the results of the proposed method produce the best overall resolution, contrast and image color.

B. OBJECTIVE EVALUATION

Subjective evaluation inevitably has a certain one-sidedness due to the focus of the effects that vary with different methods. Therefore, objective evaluation is used to further evaluate the various methods described in this paper [29]. In studying the dehazing effect, Hautière's blind evaluation method based on the visible edge contrast is well known [36]–[38].

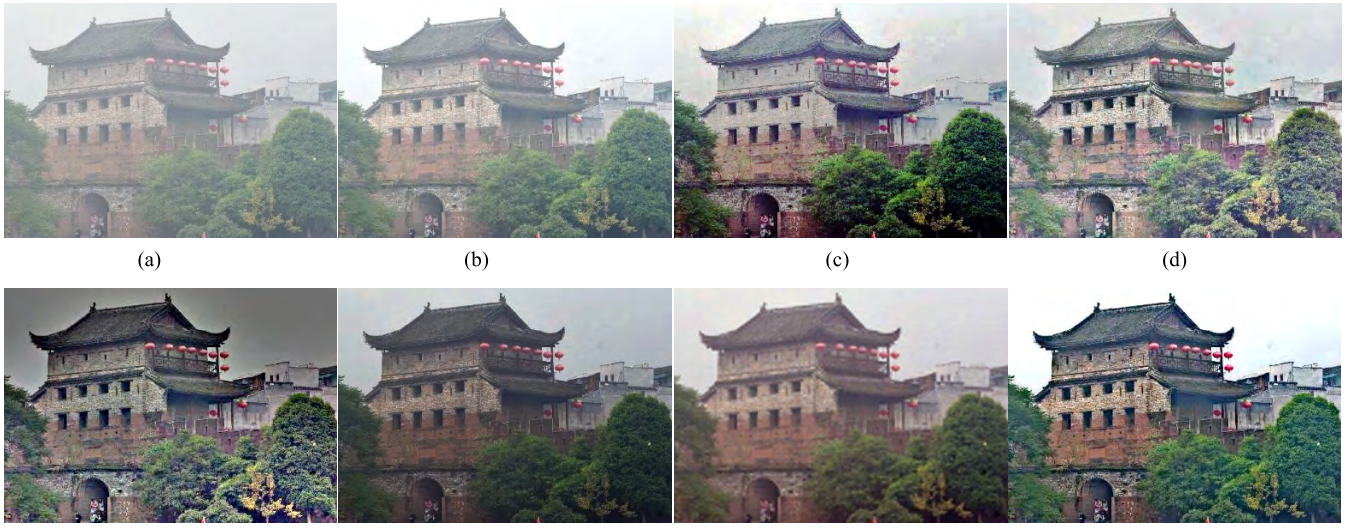

FIGURE 10. Comparison of the proposed method with alternative image-enhancement-based methods. (a) Hazy image. (b) Contrast stretching. (c) Histogram equalization. (d) AHE. (e) Retinex. (f) Homomorphic filtering. (g) Wavelet transform. (h) Proposed method.

TABLE 1. Objective evaluation.

Indexes \ Methods		Fattal's method	He's method	Kim's method	Zhu's method	Cai's method	Proposed
Pumpkins	e	0.1406	0.2808	0.1614	0.2215	0.1441	**0.2906**
	σ	0.0007	**0**	0.0044	**0**	0.0012	**0**
	$\bar{r}$	1.7432	0.6184	1.6947	1.2831	1.2859	**2.0309**
Cones	e	0.2463	**0.2941**	0.1520	0.2441	0.1390	0.1943
	σ	**0**	**0**	0.0039	**0**	0	**0**
	$\bar{r}$	1.9685	1.5774	1.8349	1.3111	1.2823	**2.0557**
Hill	e	0.0863	0.1425	0.0724	0.1231	0.0082	**0.2232**
	σ	0.0011	0.0001	0.0039	**0**	0.0179	**0**
	$\bar{r}$	1.2152	1.3133	1.6529	1.1759	1.1129	**1.7427**
Mountain	e	0.1011	**0.1736**	0.0839	0.0997	0.1115	0.1104
	σ	0.0934	0.0007	0.0057	0.0001	0.0040	**0**
	$\bar{r}$	1.7173	1.1481	1.4660	1.2131	1.1876	**1.7201**
People	e	0.2668	0.3538	0.3030	0.2157	0.1894	**0.3637**
	σ	0.1723	0.0000	0.0144	0.0001	0.0011	**0**
	$\bar{r}$	1.2222	1.0512	1.5364	1.2035	1.0783	**2.1207**

This method evaluates the contrast enhancement of each image detail before and after the dehazing. It objectively describes the quality of the image using three indicators (the new visible edge ratio e, the visible edge normalized gradient $\bar{r}$, and the percentage of saturated black or white pixels σ). The quantification is as follows:

$$e = \frac{n_r - n_0}{n_0} \tag{28}$$

$$\bar{r} = \exp\left(\frac{1}{n_r}\sum_{P_i \in \psi_r} \log r_i\right) \tag{29}$$

$$\sigma = \frac{n_s}{\dim_x \times \dim_y} \tag{30}$$

where n_0 and n_r are the numbers of visible edges of the image before and after the dehazing, respectively; Ψ_r is the set of visible edges for the dehazed image; P_i are the pixels on the visible edge; r_i is the ratio of the Sobel gradient at P_i and the corresponding point of the original image; n_s is the number of saturated black and white pixels; and $\dim_x$ and $\dim_y$ represent the width and height of the image, respectively. A larger e and $\bar{r}$ and smaller σ correspond to a higher quality of the restored image. The comparative data are shown in Table I.

Table I and Figure 11 indicate that the proposed method is superior to Fattal's method, He's method, Kim's method, Zhu's method and Cai's method for both $\bar{r}$ and σ. Although the performance of e on the second image is slightly inferior

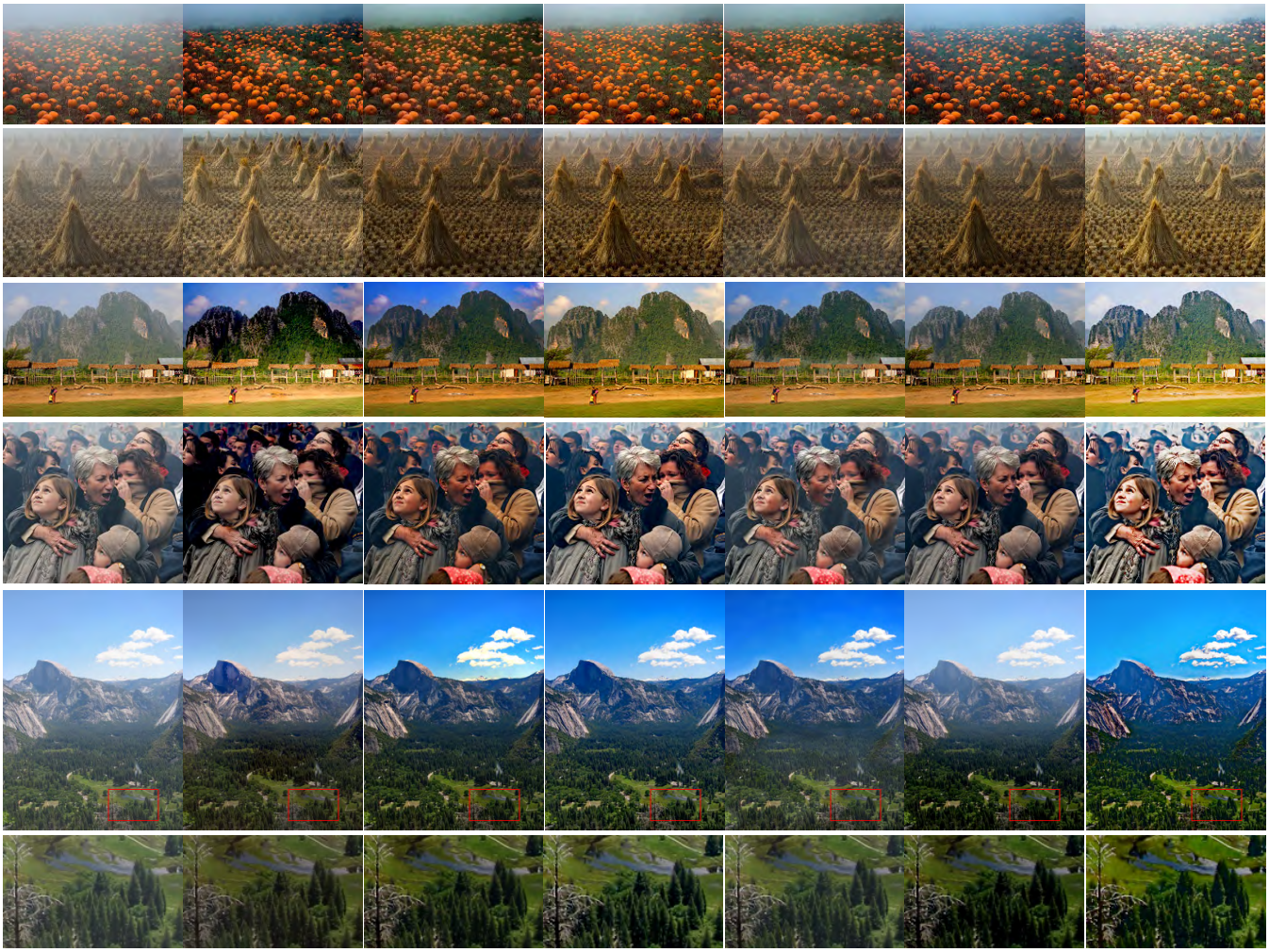

FIGURE 11. Comparison of the proposed method with various image-restoration-based methods. (a) Hazy images. (b) Fattal's method. (c) He's method. (d) Kim's method. (e) Zhu's method. (f) Cai's method. (g) Proposed method.

to that of He's method, the overall effect is a significant improvement and is generally superior to that of the other methods.

C. COMPUTATIONAL COMPLEXITY

To verify the advantages of the proposed method with respect to the processing speed, we tested images with different sizes. In this approach, each image is tested 20 times, and the average value is taken as the output. The experimental images are the eight images in Figure 9, and the computing times are shown in Table II. As the size of the image increases, the computing time correspondingly increases. For the 240,000-pixel image 'Street,' the proposed method requires only 19.9 ms of processing time. The 344,800-pixel image 'City' requires only 28.7 ms, which is sufficiently fast to be used in real-time systems.

We also used images of different sizes to compare the proposed method with He's method [15], [27], Tarel and Hautiere's [16] method, Meng *et al.*'s [21] method, Zhu *et al.*'s [24] method, and Cai *et al.*'s [39] method. The comparative data are shown in Table III, where He1 is the DCP + soft-matting method [15], He2 is the

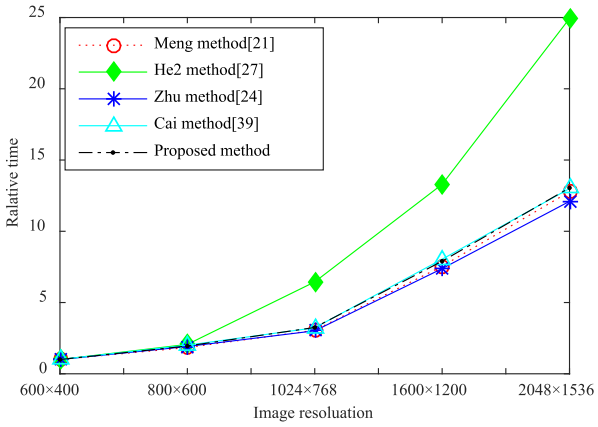

FIGURE 12. The relative speed of variation for increasing image sizes.

TABLE 2. Computational time for different sized images (unit: MS).

Images	'Street'	'Mountain'	'Cannon'	'Building'	'Toys'	'Road'	'City'	'Stadium'
Size	600×400	384×512	600×450	450×600	360×500	400×600	431×800	318×984
Time	19.9	16.8	23.0	22.4	15.5	20.0	28.7	26.8

TABLE 3. Comparison of the running time for different image-processing methods (unit: s).

Resolution	Fattal [14]	Tarel and Hautiere [16]	Meng *et al.* [21]	He *et al.* [27]	Zhu *et al.* [24]	Cai *et al.* [39]	Proposed
600×400	21.763	7.656	1.243	0.584	0.887	2.130	0.020
800×600	47.926	23.147	2.290	1.205	1.699	4.275	0.039
1024×768	83.776	56.873	3.796	3.766	2.675	6.876	0.065
1600×1200	out of memory	303.153	9.380	7.765	6.546	17.125	0.158
2048×1536	out of memory	721.632	15.885	14.561	10.732	27.684	0.261

FIGURE 13. Results of dehazing from video sequences. (a) 5^{th} frame. (b) 30^{th} frame. (c) 55^{th} frame. (d) 80^{th} frame. (e) 105^{th} frame.

DCP + guided-filtering method [27], and the window size of DCP is 15 × 15 pixels. For consistent comparison, all programs are compiled using MATLAB 2014b. Table I shows that the He1 method [15] has the lowest computational efficiency for the case of a single image, primarily because soft matting involves a large sparse linear system with high computational complexity restricted to processing only smaller images. Tarel and Hautiere's [16] method is optimized by the median filter method, but the computational complexity of the method increases rapidly as the image size increases. The He2 method [27] used a guided filter instead of the soft matting approach used in He1. The run-times are optimized, and the speed is greatly improved so that large-scale images can be processed. The efficiency of Zhu *et al.*'s [24] method and Meng *et al.*'s [21] method are similar to that of the He2 method. Zhu's method uses a linear

FIGURE 14. Comparison of images before and after dehazing. (a) Area 1. (b) Dehazed area 1. (c) Area 2. (d) Dehazed area 2. (e) Area 3. (f) Dehazed area 3.

model and guided filtering, enabling faster operation. Our proposed method uses a high-speed averaging filter, which runs faster than the above methods. For the 2048×1536 pixel image, only 0.26 s processing time is required, which is 1/40 of Zhu *et al.*'s [24] method, 1/61 of Meng *et al.*'s [21] method and 1/106 of Cai *et al.*'s [39] method. In summary, the proposed method is significantly faster than traditional image-processing approaches.

The relative time approach was employed to compare the increase in computing time for each method with increasing image size. Assuming that the processing time of the smallest image is t_1, the relative operation time is expressed as

$$T_r = t_n/t_1 \tag{31}$$

where n is the image index, which increases with the size of the test images. The relative time curves for Meng *et al.*'s [21] method, He *et al.*'s [27] method, Zhu *et al.*'s [24] method, Cai *et al.*'s [39] method and the proposed method are shown in Figure 12.

With increasing image size, the relative processing time for the various methods monotonically increases. The He2 method shows the maximum slope. Zhu's method, Meng's method, Cai's method and the proposed method have similar rates of change. (Note that the values for Cai's method and the proposed method are essentially the same.) Therefore, our method is appropriate for the processing of large images. We conclude that our proposed method offers high efficiency of implementation.

A 600 × 400 pixel image requires only 20ms in the MATLAB 2014b environment, which meets the requirements of real-time video processing. Figure 13 shows the dehazing result of randomly selected partial frames from two hazy monitoring videos [22]. The odd rows are 5, 30, 55, 80, and 105 frames of the original hazy video sequence, and the even rows are the corresponding dehazing results of the proposed method. Figure 14 shows an enlarged image before and after dehazing. The proposed method can effectively accommodate hazy videos with limited distortion, which shows the robustness and practicality of the algorithm.

V. CONCLUSIONS

To improve the computational complexity of dehazing algorithms, a fast single-image dehazing method is proposed based on the DCP theory and gray projection. The optimized average filtering method and box filter acceleration strategy are used to accommodate high-resolution and hazy images and videos in real-time systems. An atmospheric light acquisition method is designed based on the regional projection, and an amendment strategy for large white areas is proposed. Finally, an adaptive adjustment method based on human visual perception is proposed to solve the problem of low brightness in restored images. Relative to current state-of-the-art algorithms, it is concluded that the images restored from the proposed method appear clearer and more natural. The algorithm has a wide range of applicability to ensure the balance of quality and the speed of the image restoration and can be used in video systems. The key limitation of the proposed algorithm is that shadows appear at the edges of the dehazed image. Retaining the details and achieving edge smoothing is the subject of planned future work.

REFERENCES

[1] H. Lu *et al.*, "Depth map reconstruction for underwater Kinect camera using inpainting and local image mode filtering," *IEEE Access*, vol. 5, pp. 7115–7122, Apr. 2017.
[2] Y. Liu, H. Li, and M. Wang, "Single image dehazing via large sky region segmentation and multiscale opening dark channel model," *IEEE Access*, vol. 5, pp. 8890–8903, May 2017.
[3] T. K. Kim, J. K. Paik, and B. S. Kang, "Contrast enhancement system using spatially adaptive histogram equalization with temporal filtering," *IEEE Trans. Consum. Electron.*, vol. 44, no. 1, pp. 82–87, Feb. 1998.
[4] T. J. Cooper and F. A. Baqai, "Analysis and extensions of the Frankle-McCann Retinex algorithm," *J. Electron. Imag.*, vol. 13, no. 1, pp. 85–92, Jan. 2004.
[5] M.-J. Seow and V. K. Asari, "Ratio rule and homomorphic filter for enhancement of digital colour image," *Neurocomputing*, vol. 69, nos. 7–9, pp. 954–958, Mar. 2006.
[6] S. Dippel, M. Stahl, R. Wiemker, and T. Blaffert, "Multiscale contrast enhancement for radiographies: Laplacian pyramid versus fast wavelet transform," *IEEE Trans. Med. Imag.*, vol. 21, no. 4, pp. 343–353, Apr. 2002.
[7] J. P. Oakley and B. L. Satherley, "Improving image quality in poor visibility conditions using a physical model for contrast degradation," *IEEE Trans. Image Process.*, vol. 7, no. 2, pp. 167–179, Feb. 1998.
[8] S. G. Narasimhan and S. K. Nayar, "Interactive (de) weathering of an image using physical models," in *Proc. IEEE Workshop Color Photometric Methods Comput. Vis.*, Paris, France, Oct. 2003, pp. 1–8.
[9] N. Hautière, J.-P. Tarel, and D. Aubert, "Towards fog-free in-vehicle vision systems through contrast restoration," in *Proc. IEEE Conf. Comput. Vis. Pattern Recognit.*, Minneapolis, MN, USA, Jun. 2007, pp. 1–8.
[10] J. Kopf *et al.*, "Deep photo: Model-based photograph enhancement and viewing," *ACM Trans. Graph.*, vol. 27, no. 5, p. 116, 2008.
[11] Y. Y. Schechner, S. G. Narasimhan, and S. K. Nayar, "Instant dehazing of images using polarization," in *Proc. IEEE Conf. Comput. Vis. Pattern Recognit.*, Kauai, HI, USA, Dec. 2001, pp. 325–332.
[12] S. K. Nayar and S. G. Narasimhan, "Vision in bad weather," in *Proc. 7th IEEE Int. Conf. Comput. Vis.*, Kerkyra, Greece, Sep. 1999, pp. 820–827.
[13] R. T. Tan, "Visibility in bad weather from a single image," in *Proc. IEEE Conf. Comput. Vis. Pattern Recognit.*, Anchorage, AK, USA, Jun. 2008, pp. 1–8.

[14] R. Fattal, "Single image dehazing," *ACM Trans. Graph.*, vol. 27, no. 3, p. 72, Aug. 2008.
[15] K. He, J. Sun, and X. Tang, "Single image haze removal using dark channel prior," *IEEE Trans. Pattern Anal. Mach. Intell.*, vol. 33, no. 12, pp. 2341–2353, Dec. 2011.
[16] J.-P. Tarel and N. Hautière, "Fast visibility restoration from a single color or gray level image," in *Proc. IEEE 12th Int. Conf. Comput. Vis.*, Kyoto, Japan, Sep. 2009, pp. 2201–2208.
[17] L. Kratz and K. Nishino, "Factorizing scene albedo and depth from a single foggy image," in *Proc. IEEE 12th Int. Conf. Comput. Vis.*, Kyoto, Japan, Sep. 2009, pp. 1701–1708.
[18] C. O. Ancuti and C. Ancuti, "Single image dehazing by multi-scale fusion," *IEEE Trans. Image Process.*, vol. 22, no. 8, pp. 3271–3282, Aug. 2013.
[19] Z. Wang and Y. Feng, "Fast single haze image enhancement," *Comput. Elect. Eng.*, vol. 40, no. 3, pp. 785–795, Apr. 2014.
[20] K. B. Gibson and T. Q. Nguyen, "Fast single image fog removal using the adaptive Wiener filter," in *Proc. IEEE Int. Conf. Image Process.*, Melbourne, VIC, Australia, Sep. 2013, pp. 714–718.
[21] G. Meng, Y. Wang, J. Duan, S. Xiang, and C. Pan, "Efficient image dehazing with boundary constraint and contextual regularization," in *Proc. IEEE Int. Conf. Comput. Vis.*, Sydney, NSW, Australia, Dec. 2013, pp. 617–624.
[22] J.-H. Kim, W.-D. Jang, J.-Y. Sim, and C.-S. Kim, "Optimized contrast enhancement for real-time image and video dehazing," *J. Vis. Commun. Image Represent.*, vol. 24, no. 3, pp. 410–425, Apr. 2013.
[23] R. Fattal, "Dehazing using color-lines," *ACM Trans. Graph.*, vol. 34, no. 1, p. 13, Dec. 2014.
[24] Q. Zhu, J. Mai, and L. Shao, "A fast single image haze removal algorithm using color attenuation prior," *IEEE Trans. Image Process.*, vol. 24, no. 11, pp. 3522–3533, Nov. 2015.
[25] J. Yu, C. Xiao, and D. Li, "Physics-based fast single image fog removal," in *Proc. IEEE 10th Int. Conf. Signal Process.*, Beijing, China, Oct. 2010, pp. 1048–1052.
[26] C.-H. Yeh, L.-W. Kang, M.-S. Lee, and C.-Y. Lin, "Haze effect removal from image via haze density estimation in optical model," *Opt. Exp.*, vol. 21, no. 22, pp. 27127–27141, Nov. 2013.
[27] K. He, J. Sun, and X. Tang, "Guided image filtering," *IEEE Trans. Pattern Anal. Mach. Intell.*, vol. 35, no. 6, pp. 1397–1409, Jun. 2013.
[28] A. K. Tripathi and S. Mukhopadhyay, "Single image fog removal using anisotropic diffusion," *IET Image Process.*, vol. 6, no. 7, pp. 966–975, Oct. 2012.
[29] Y. H. Shiau, H. Y. Yang, P. Y. Chen, and Y. Z. Chuang, "Hardware implementation of a fast and efficient haze removal method," *IEEE Trans. Circuits Syst. Video Technol.*, vol. 23, no. 8, pp. 1369–1374, Aug. 2013.
[30] S.-C. Huang, B.-H. Chen, and W.-J. Wang, "Visibility restoration of single hazy images captured in real-world weather conditions," *IEEE Trans. Circuits Syst. Video Technol.*, vol. 24, no. 10, pp. 1814–1824, Oct. 2014.
[31] W. Wang, X. Yuan, X. Wu, and Y. Liu, "Fast image dehazing method based on linear transformation," *IEEE Trans. Multimedia*, vol. 19, no. 6, pp. 1142–1155, Jun. 2017.
[32] P. Viola and M. Jones, "Rapid object detection using a boosted cascade of simple features," in *Proc. IEEE Comput. Soc. Conf. Comput. Vis. Pattern Recognit. (CVPR)*, Kauai, HI, USA, Dec. 2001, pp. I-511–I-518.
[33] J. Jiang, T. Hou, and M. Qi, "Improved algorithm on image haze removal using dark channel prior," *J. Circuits Syst.*, vol. 16, no. 2, pp. 7–12, 2011.
[34] W. Wang, X. Yuan, X. Wu, and Y. Liu, "Dehazing for images with large sky region," *Neurocomputing*, vol. 238, pp. 365–376, May 2017.
[35] J. Shen, "On the foundations of vision modeling: I. Weber's law and Weberized TV restoration," *Phys. D, Nonlinear Phenom.*, vol. 175, no. 3, pp. 241–251, Feb. 2003.
[36] N. Hautière, J. P. Tarel, D. Aubert, and E. Dumont, "Blind contrast enhancement assessment by gradient ratioing at visible edges," *Image Anal. Stereol.*, vol. 27, no. 2, pp. 87–95, Apr. 2011.
[37] H. Yuan, C. Liu, Z. Guo, and Z. Sun, "A region-wised medium transmission based image dehazing method," *IEEE Access*, vol. 5, pp. 1735–1742, Jan. 2017.
[38] W. Wang, X. Wu, T. Ji, and L. Feng, "Gray projection for single image dehazing," in *Proc. Youth Acad. Annu. Conf. Chin. Assoc. Autom.*, Nanjing, China, 2018, pp. 1–4.
[39] B. Cai, X. Xu, K. Jia, C. Qing, and D. Tao, "DehazeNet: An end-to-end system for single image haze removal," *IEEE Trans. Med. Imag.*, vol. 25, no. 11, pp. 5187–5198, Nov. 2016.

WENCHENG WANG (M'16) received the Ph.D. degrees in pattern recognition and intelligent system from the Shandong University, Jinan, in 2011. He is currently a Professor with the College Of Information and Control Engineering, Weifang University. From 2015 to 2016, he was a Visiting Scholar with the University of North Texas, where he was involved in the research of computer vision and automatic detection technology, especially on image dehazing. His group has published and authored over 40 papers on academic journals and conferences. His main research interests include computer vision, pattern recognition, and intelligent computing. He received the Young researcher's Award of Weifang University in 2010. He is currently serving as an Associate Editor for the International Journal *Transactions of the Institute of Measurement and Control*.

FALIANG CHANG was born in 1965. He received the B.S. and M.S. degree from Shandong University, China, in 1989 and 1991, respectively. From 2008 to 2009, he was a Visiting Scholar with Michigan State University, USA. He is currently a Professor and a Doctorate Supervisor with Shandong University. He has published two books and over100 papers, and holds a national patent. His main research interests include digital signal processing, computer vision, pattern recognition, and visual tracking.

TAO JI was born in Weifang, Shandong, China, in 1975. He received the Ph.D. degree from Shandong University in 2006. Since 2006, he has been with the College of Information and Control Engineering, Weifang University, where he is currently a Professor. He has published and authored over 30 papers on academic journals and conferences. His research interests include intelligent control and information processing.

XIAOJIN WU received the Ph.D. degree in 2011. He is currently with the College of Information and Control Engineering, Weifang University, China. He has published and authored over 10 papers on academic journals and conferences. His main research interests include intelligent system and image processing.